



**TEST CASE DEFINITION FOR NUMERICAL
REBUILDING WITHIN THE EUROPEAN
ABLATION WORKING GROUP
CONTRACT 067/2007**

Philippe Reynier – Guillaume Chambre

**ISA TN-04-2007
OCTOBER 2007**

Ingénierie et Systèmes Avancés
Technopole Bordeaux Technowest
Tour C - Domaine James Watt
19, allée James Watt
F-33700 Mérignac

Tel: +33 (0) 556479274
Fax: +33 (0) 556473148

| | |
|------------|----------------------------|
| Visa | Ph Reynier |
| Version n° | 2 |
| Date | 16 th Oct. 2007 |

| CONTENTS | PAGE N° |
|---|----------------|
| 1 INTRODUCTION..... | 6 |
| 2 INPUT LIST | 7 |
| 2.1 Material properties list | 7 |
| 2.2 Flow conditions | 7 |
| 2.3 Other relevant data | 7 |
| 3 TEST CASE 1 – ATJ GRAPHITE | 9 |
| 3.1 Background..... | 9 |
| 3.2 Objective..... | 9 |
| 3.3 Inputs | 10 |
| 3.3.1 Geometry | 10 |
| 3.3.2 Test Matrix | 10 |
| 3.3.3 Experimental Data | 11 |
| 3.3.4 Material properties | 12 |
| 3.3.5 Oxidation and Sublimation | 14 |
| 3.3.6 Chemical Kinetics | 15 |
| 3.4 Output | 15 |
| 4 TEST CASE 2 – DEGRADATION OF CARBON PHENOLIC..... | 17 |
| 4.1 Background..... | 17 |
| 4.2 Objective..... | 17 |
| 4.3 Inputs | 17 |
| 4.3.1 Geometry | 18 |
| 4.3.2 Test Matrix | 18 |
| 4.3.3 Experimental Data | 21 |
| 4.3.4 Material properties | 21 |
| 4.3.5 Chemical Kinetics | 24 |
| 4.4 Output | 24 |
| 5 ANNEXES..... | 25 |
| 5.1 Critical Literature Review of ATJ Graphite's data | 25 |
| 5.2 Maah's analysis of his own experiments | 26 |
| 5.3 Critical Literature Review for Carbon phenolic | 27 |
| 5.4 Sutton's experiments..... | 28 |
| 5.5 Sutton's numerical rebuilding | 31 |
| 6 REFERENCES..... | 32 |

LIST OF FIGURES

| | |
|---|----|
| Figure 1: Dimensionless ablation rate for classical carbon in air with equilibrium assumption [2] as function of temperature. | 9 |
| Figure 2: Schematic diagram of test samples. | 10 |
| Figure 3: Conical shape of the sample after the test with a pressure of 15 atm. | 11 |
| Figure 4: Surface temperature and mass-loss-rate as function of stagnation pressure in Maahs experiments. | 12 |
| Figure 5: Distributions of specific heat and thermal conductivity as function of temperature for ATJ graphite. | 13 |
| Figure 6: Geometry of the hemispheric samples [15]. | 18 |
| Figure 7: Recession and surface temperature as function of time for the test with air at the stagnation pressure of 0.31 atmosphere. | 19 |
| Figure 8: Recession and surface temperature as function of time for the test with air at the stagnation pressure of 10.91 atmospheres. | 20 |
| Figure 9: Distributions of specific heat and thermal conductivity as function of temperature for Narmco 4028 (virgin material). | 23 |
| Figure 10: Distributions of specific heat and thermal conductivity as function of temperature for Narmco 4028 (char material) measured in [16]. | 23 |
| Figure 11: Distribution of the specific heat of the pyrolysis gases as function of temperature for Narmco 4028 computed by Sutton. | 23 |
| Figure 12: Char removal of an hemispheric model for a test a 11.26 atm. | 31 |
| Figure 13: Distributions of specific heat and thermal conductivity as function of temperature used by Sutton for Narmco 4028 (virgin material). | 31 |
| Figure 14: Distributions of specific heat and thermal conductivity as function of temperature used by Sutton for Narmco 4028 (char material). | 32 |

LIST OF TABLES

| | |
|--|----|
| Table 1: Maahs's experimental conditions [6]. | 11 |
| Table 2: Maahs's experimental results. | 12 |
| Table 3: Properties of ATJ graphite used in Maahs's experiment. | 13 |
| Table 4: Values of the heat capacity and thermal conductivity measured by Wakefield & Peterson. | 14 |
| Table 5: Coefficients for the interpolation of the specific heat and the thermal conductivity for a range of temperatures from 400 K up to 4000 K. | 14 |
| Table 6: Values of the constants a_1 to a_6 used to calculate the oxidation rate. | 15 |
| Table 7: Test Case matrix from Sutton's experiments [15]. | 18 |
| Table 8: Sutton's test results [15]. | 19 |
| Table 9: Time evolution of the surface temperature for the test with air at the stagnation pressure of 0.31 atmosphere. | 20 |
| Table 10: Time evolution of the surface temperature for the test with air at the stagnation pressure of 10.91 atmospheres. | 20 |
| Table 11: Elemental composition of Narmco 4028. | 21 |
| Table 12: Properties of carbon-phenolic Narmco 4028 used by Sutton. | 21 |
| Table 13: Values of the heat capacity for the Narmco 4028 (virgin). | 22 |
| Table 14: Values of the heat capacities for the char material and the pyrolysis gas for the Narmco 4028. | 22 |
| Table 15: Values of the thermal conductivity measured in the fibre direction for the virgin material [16]. | 22 |
| Table 16: Values of the thermal conductivity measured in the fibre direction for the char material [16]. | 22 |
| Table 17: Properties for the char material used by Sutton. | 24 |
| Table 18: Values of the constants, A, B and C for the slower and faster rates respectively. | 27 |
| Table 19: Sutton's test experimental conditions [15]. | 29 |
| Table 20: Sutton's test results | 30 |
| Table 10: Properties for the char material used by Sutton. | 32 |

1 INTRODUCTION

In 2005 the European Space Agency has settled, in cooperation with other agencies, research institutes and industry, a European Ablation Working Group (EAWG) [1]. Two of the major objectives of the EAWG are the establishment of a common material database and the improvement of the numerical modelling capabilities. In order to fulfil these objectives, a set of test cases for numerical rebuilding [2] has been discussed and agreed in the 2nd meeting of the EAWG held at ESTEC on 16th May 2006.

The need for additional material tests in plasma facilities has been anticipated. During the meeting on 16th May 2006, an opportunity was offered by CIRA to perform material sample testing in SCIROCCO, this opportunity was confirmed during the 3rd meeting held in Bordeaux on 25-26th January 2007.

During this 3rd meeting, a refinement of these test cases was presented [3] with the preliminary definition of a potential test set-up and a list of material properties and flow characteristics required for the numerical rebuilding. The outcome of a preliminary literature review focusing on the available data in the perspective of the test case definition was also presented.

Finally, two test cases have been selected. The first one is the rebuilding of experiments performed for graphite, while the material chosen for the second test case is the carbon phenolic. These test cases are defined in the following, their description focuses on the numerical rebuilding using existing experimental data from the literature in order to provide the booklets to organize the 1st Ablation Workshop.

2 INPUT LIST

The numerical rebuilding of experiments and/or flight data requests the knowledge of a set of material properties as well as flow conditions. From software available at ISA [4,5] a set of the different data needed for the numerical work has been derived. This input list was presented and agreed during the 3rd EAWG meeting.

2.1 Material properties list

A generic list of material characteristics is provided below. This list is not exhaustive, but intends to identify the material parameters required for the numerical rebuilding. Note also that the applicability differs, depending on the numerical code:

- Chemical composition;
- Resin volume fraction;
- Crystalline structure;
- Structural properties;
- Material densities of virgin and charred materials;
- Surface emissivity of virgin and charred materials;
- Heat of ablation and ablation temperature;
- Thermal conductivity of virgin and charred materials;
- Specific heats of virgin and charred materials;
- For each ablator component: charred and virgin densities and activation temperature [4];
- Heat of formation of pyrolysis gas and reference temperature;
- Pyrolysis gas enthalpy;
- Temperature of pyrolysis gas;
- Composition of pyrolysis gas.

2.2 Flow conditions

The flow conditions required for the rebuilding are the following:

- Atmospheric density;
- Atmospheric pressure;
- Atmosphere composition;
- Surface temperature;
- Surface pressure;
- Cold wall convective heat-flux;
- Radiative heat-flux;
- Stagnation pressure;
- Wall gas enthalpy.

2.3 Other relevant data

- Storage conditions (if applicable);

- Initial material thickness;
- Blowing efficiency of pyrolysis gases in reducing convective heat-flux (convective blockage).

3 TEST CASE 1 – ATJ GRAPHITE

3.1 Background

A simple ablating material involving no physical or chemical transformation below the surface is the most logical first step for investigating surface phenomena without additional complexity. Due to its simple chemical composition, the absence of pyrolysis, and a reasonable number of studies reported in the literature, a rough surface graphite has been selected during the 3rd meeting held on January 25-26th 2007: **ATJ Graphite**.

If a variety of flow conditions (laminar, turbulent, radiation, steady state or time dependant conduction) can be imagined, a simple laminar case for air without radiative heating has been retained.

Test Case 1 is initiated with a rough surface graphite. Further extension of this test case could be to include a modern fine grain smooth graphite but still for laminar flow conditions. Even in the laminar regime, some phenomenon such as the surface nitridation are poorly understood. As shown in Figure 1, graphite ablation is, increasing surface temperature, dominated by surface kinetics, then diffusion and finally sublimation.

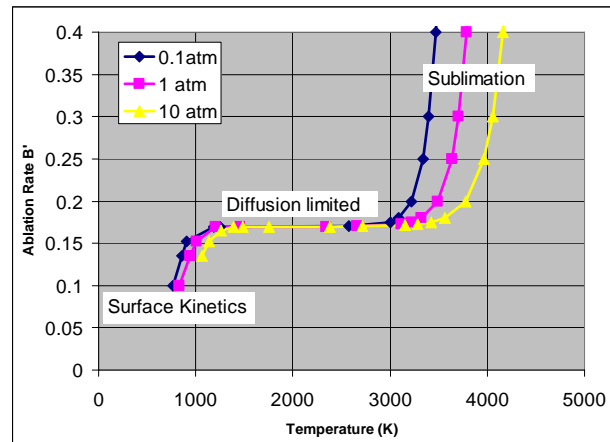


Figure 1: Dimensionless ablation rate for classical carbon in air with equilibrium assumption [2] as function of temperature.

A critical review of the available data from the literature on polycrystalline graphite has shown that the investigations of Maahs [6] appear to be the most complete. However, a gap exists in the experimental data with little material covering the surface kinetics regime. This could be filled by defining future experiments to be performed in the frame of the working group activities.

3.2 Objective

The objective of the Test Case 1 is to rebuild the experiments of Maahs [6] performed with polycrystalline graphite. The main outcome will be the prediction of the ablation rate versus entry dynamic conditions (cold wall heat flux and wall pressure). From the experimental results a matrix of computational conditions has been defined to cover, as far as possible, the classical carbon ablation regime covering oxidation, diffusion and sublimation as shown in Figure 1 for the ranges of interest for

the EAWG.

The main objective of the test case will be to demonstrate the numerical capabilities of the solvers to predict the mass-loss-rate and total recession as function of stagnation pressure and surface temperature. This, for a wide range of physical conditions and a stagnation point configuration. Computations can be uncoupled which requires a knowledge of the surface temperature or coupled, depending only on test conditions.

3.3 Inputs

The inputs have been defined using the experimental data for test conditions and material properties available in [6]. The input parameters have been chosen to insure the best coverage of the different carbon ablation regimes (oxidation, diffusion limiting and sublimation) shown in Figure 1.

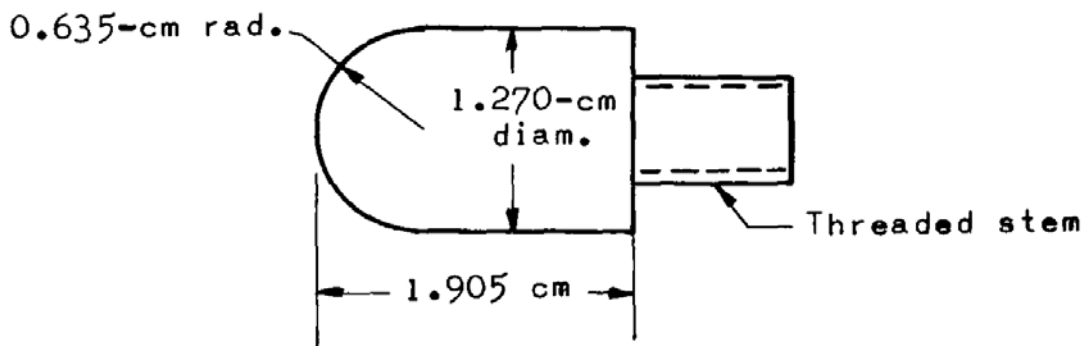


Figure 2: Schematic diagram of test samples.

3.3.1 Geometry

The hemispheric geometry of the test sample is shown in Figure 2. It is a hemispheric cylinder with a diameter of 1.27 cm. The sample is 1.905 cm long with a nose radius of 0.635 cm. The specimen was machined with the across-grain direction parallel to the axis of the specimen. That is, the direction of the lowest thermal conductivity.

The sample size is small but this allows to reproduce entry conditions in terms of heat-flux and pressure characteristics of an Earth super orbital re-entry. Due to the small size for such samples, the boundary effects are important. As a consequence for the numerical rebuilding, stagnation point calculations will be considered.

3.3.2 Test Matrix

The experimental campaigns carried out by Maahs for the polycrystalline graphite were conducted for a wide range of experimental conditions reported in Table 1. Tests were performed for an air atmosphere in four different facilities for stagnation pressures from 0.035 up to 15 atm and nominal enthalpies from 2.55 up to 34.9 MJ/kg. The corresponding range of surface temperature was between 2000 and 3000 K. The values of surface temperature and cold wall heat flux are reported in Table 2.

There was a low radiation environment for the tests without significant radiative heating rate.

According to Figure 1, using these different ranges of pressure and enthalpy, both sublimation and diffusion limited modes are covered. Unfortunately, the surface kinetics regime is not obtained for these conditions due to a too high surface temperature.

| Stagnation pressure (atm) | Duration (s) | Nominal total enthalpy (MJ/kg) | Free-stream pressure (atm) | Mach number | Facility |
|---------------------------|--------------|--------------------------------|----------------------------|-------------|----------|
| 0.035 | 60 | 34.9 | 0.0002 | 9 | HEAT |
| 0.6 | 45 | 23 | 0.23 | 4.3 | HAHT |
| 2.2 | 60 | 4.63 | 0.13 | 4 | HAHT |
| 5.6 | 30 | 2.36 | 0.66 | 2.5 | AHMJ |
| 15 | 20 | 2.55 | 2.43 | 2.1 | CHT |

Table 1: Maahs's experimental conditions [6].

The test performed for a stagnation pressure of 15 atm have shown the presence of mechanical erosion. As show in Figure 3, at the end of the test, the sample geometry was not hemispheric but conical. This conical shape, with an angle of 50°, reflects the presence of a transitional flow: only a small part close to the stagnation point remains hemispheric. Since Test Case 1 was initially restricted to laminar flow conditions, the test performed for a stagnation pressure of 15 atm will not be included.

To resume, the test matrix is based on the tests performed at stagnation pressure of: 0.035, 0.6, 2.2 and 5.6 in Table 1. The last case at 15 atm is optional and is not part of Test Case 1.



Figure 3: Conical shape of the sample after the test with a pressure of 15 atm.

3.3.3 Experimental Data

All test data was obtained at stagnation point for steady state conditions. The convective cold wall heat flux was related to enthalpy by the equation of Fay and Riddell [7]. The parameters selected for

assessing ablation performance were the total recession as function of test duration, the mass-loss-rate and the surface temperature.

Measurements were performed for the different test conditions of Table 1 for the surface temperature (at steady-state conditions), the total recession and the mass-loss-rate, they are reported in Table 2. The distributions of the mass-loss-rate and surface temperature as function of the stagnation pressure are plotted in Figure 4.

| Stagnation pressure (atm) | Experimental results | | | |
|---------------------------|-----------------------------------|----------------------|---|---------------------|
| | Heating rate (W/cm ²) | Total recession (cm) | Mass-loss rate (kg.m ⁻² .s ⁻¹) | Surface temperature |
| 0,035 | 760 | 0,1612 | 0,04013 | 2485 |
| 0,6 | 2073 | 0,5305 | 0,20050 | 3376 |
| 2,2 | 761 | 0,5016 | 0,16045 | 2076 |
| 5,6 | 570 | 0,4259 | 0,29906 | 2085 |
| 15 | 1011 | 1,0483 | 0,54860 | 2579 |

Table 2: Maahs's experimental results.

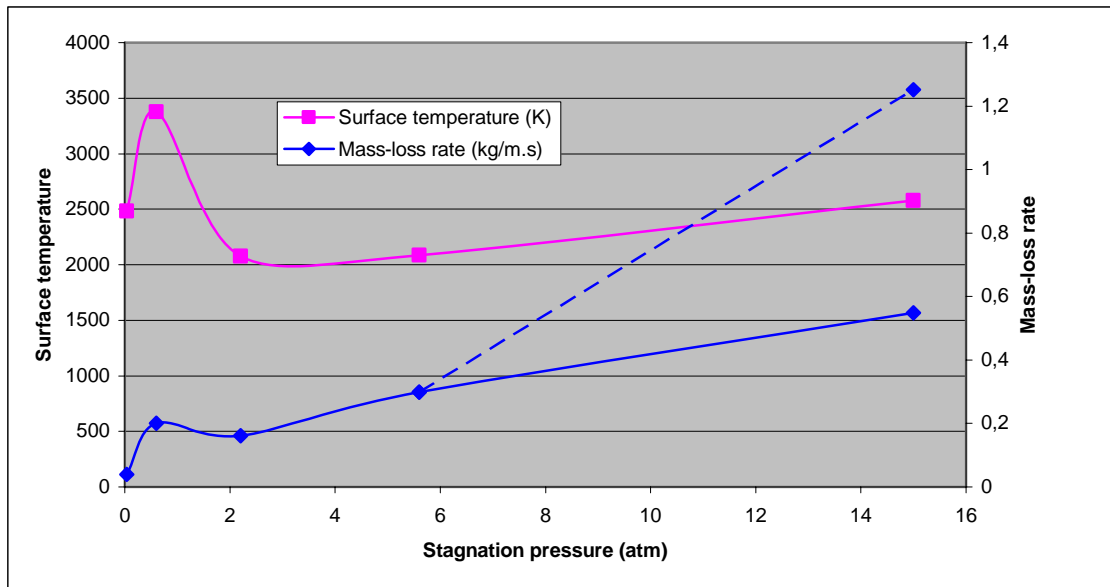


Figure 4: Surface temperature and mass-loss-rate as function of stagnation pressure in Maahs experiments.

3.3.4 Material properties

For his experimental campaigns, Maahs [6] had tested four different graphite, among them, ATJ graphite, selected for this study, was supplied by the Union Carbide Corporation. ATJ graphite is an polycrystalline and anisotropic graphite. The anisotropy ratio of ATJ graphite is 1/2. This ratio

corresponds to the relative number of crystalline faces lying in a plane parallel to the across-grain direction of the graphite to those lying in the perpendicular plane. The material properties of this anisotropic graphite have been gathered from the literature and incorporated in the material database presented during the 3rd EAWG meeting [8].

| Property | ATJ graphite |
|--|--------------------|
| Density (kg/m ³) | 1720 |
| Young's modulus, GN/m ² | 7.6 |
| Tensile strength, MN/ m ² | 23.4 |
| Compressive strength, MN/ m ² . | 60.7 |
| Flexural strength, MN/ m ² | 24.8 |
| Thermal conductivity, W.m ⁻¹ .K ⁻¹ | 92 |
| Thermal expansion, per K | 3.5e ⁻⁶ |
| Permeability (helium), m ² .s ⁻¹ | 5.9e ⁻⁴ |
| Emissivity | 0.94 |

Table 3: Properties of ATJ graphite used in Maahs's experiment

Some of the required material properties available from the report of Maahs [6] are presented in Table 3. They have been obtain from [6] and [9].

Other thermomechanical properties such as the specific heat and the thermal conductivity as function of the temperature can be found in [10] and [11]. The distributions of these two quantities as function of temperature are displayed in Figure 5 the corresponding values in Table 4. The figure shows a good agreement between the data of Wakefield & Peterson [10] and the NASA [11] database for the specific heat. There is a large discrepancy with a factor two at high temperature for the thermal conductivity (measured in the direction parallel to the flow).

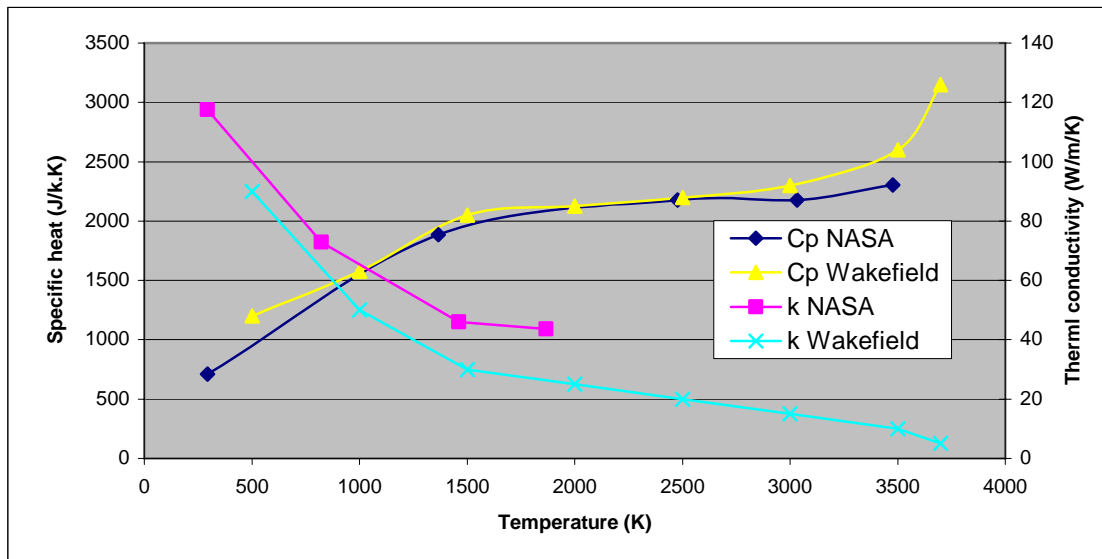


Figure 5: Distributions of specific heat and thermal conductivity as function of temperature for ATJ graphite.

Since the set of data for the thermal conductivity provided in [11] is not valid above 2000 K, the choice is done to use, for Test Case 1, the values of the thermal conductivity and heat capacity measured by

Wakefield & Peterson [10]. Other data can be used, however a set of computations (and results) with the data of Wakefield & Peterson reported in Table 4 is mandatory.

| | | | | | | | | |
|-----------|------|------|------|------|------|------|------|------|
| T | 500 | 1000 | 1500 | 2000 | 2500 | 3000 | 3500 | 3700 |
| Cp | 1200 | 1575 | 2050 | 2125 | 2200 | 2300 | 2600 | 3150 |
| k | 90 | 50 | 30 | 25 | 20 | 15 | 10 | 5 |

Table 4: Values of the heat capacity and thermal conductivity measured by Wakefield & Peterson.

From their experimental data Wakefield & Peterson [10] have extracted the following correlations providing the specific heat and the thermal conductivity as function of the temperature:

$$C_p = A_1 T^5 + A_2 T^4 + A_3 T^3 + A_4 T^2 + A_5 T + A_6 \quad (3.1)$$

$$\kappa = B_1 T^5 + B_2 T^4 + B_3 T^3 + B_4 T^2 + B_5 T + B_6 \quad (3.2)$$

The two sets of coefficients A_i and B_i are given in Table 5.

| | Coefficients | | | | | |
|------------|--------------|-------------|------------|-----------|--------|--------|
| ΔT | A_1 | A_2 | A_3 | A_4 | A_5 | A_6 |
| 300/4000 | $2e^{-14}$ | $-1e^{-10}$ | $1e^{-7}$ | $6e^{-5}$ | 0,7368 | 801,88 |
| ΔT | B_1 | B_2 | B_3 | B_4 | B_5 | B_6 |
| 300/4000 | $-4e^{-16}$ | $6e^{-12}$ | $-4e^{-8}$ | $1e^{-4}$ | 0,2185 | 171,36 |

Table 5: Coefficients for the interpolation of the specific heat and the thermal conductivity for a range of temperatures from 400 K up to 4000 K.

3.3.5 Oxidation and Sublimation

Two phenomena required to be modelled:

- Oxidation of the carbon by atomic oxygen;
- Carbon sublimation.

The correlations used by Ahn & Park [5] in KCMA have been retained. The oxidation rate of the carbon is given by:

$$R_{oxy} = \rho_s \left(a_1 + \frac{H - a_2}{a_3} e^{-a_4 + a_5 f_s - a_6 f_s^2} \right) \quad (3.3)$$

With,

$$f_s = \frac{\rho V}{\rho_s} \quad (3.4)$$

where H is the total enthalpy, ρ_s the material surface density, V the flow velocity and ρ the flow

density. The constants a_1 to a_6 are reported in Table 6.

| a_1 | a_2 | a_3 | a_4 | a_5 | a_6 |
|-------|-------|-------|-------|--------|-------|
| 0,14 | 25 | 35,5 | 4,04 | 0,5861 | 0,035 |

Table 6: Values of the constants a_1 to a_6 used to calculate the oxidation rate.

Carbon sublimates at high temperature. It is now that the sublimation product of graphite is mostly C_3 . As a consequence, the sublimation rate R_s will be modelled as in KCMA (see [12,13]),

$$R_s = \frac{1.9 \cdot 10^9}{4} \alpha_{C_3} M_{C_3} e^{\frac{-59410}{T_w}} \sqrt{\frac{8k}{\pi m_{C_3} T_w}} \quad (3.5)$$

Where T_w is the surface temperature, k the Boltzmann constant, and M_{C_3} and m_{C_3} the molar and molecular mass of C_3 respectively. α_{C_3} is given by,

$$\alpha_{C_3} = \frac{30e^{\frac{21490}{T_w}}}{1 + 30e^{\frac{21490}{T_w}}} \quad (3.6)$$

Using this modelling, surface nitridation is neglected. For the Test Case 1 computations with these different correlations are mandatory. Comparisons with other empirical or semi-empirical correlations are welcome.

3.3.6 Chemical Kinetics

For Test Case 1, mass fraction of the different component of air atmosphere (O, N, N_2 , O_2 , NO) will be considered to be at equilibrium.

For fully coupled calculations using a CFD code accounting for non equilibrium, the chemical model to be used will be the one proposed by Park et al [12].

3.4 Output

Model details should be provided when possible: i.e. underlying databases, and methodology. Assumptions made in transport properties for all methods should be stated.

The ablation process is strongly driven by the surface temperature depending on test/entry conditions. This variable depends on the coupling between the flow conditions and the material behaviour. Nevertheless, in a first step it appears suitable to displays the ablation rate as function of surface temperature and wall pressure (as done in Figure 1) and/or cold wall heat flux and wall pressure.

Outputs should contain surface species, reactions and mole fraction profiles from the surface if CFD calculations have been performed, all in Excel sheet format.

The results of the calculations for each of the mandatory cases should also be under the form of an Excel sheet containing for each case all used inputs (at least, wall heat flux and stagnation pressure) and as outputs at least mass-loss-rate, surface recession and surface temperature at steady state.

For the numerical rebuilding, surface solutions can be empirical, equilibrium/transfer coefficient, coupled boundary layer or Navier-Stokes solutions. In further activities full kinetics non-equilibrium solutions can be considered as most suitable to compare with detailed modern spectral measurements.

4 TEST CASE 2 – DEGRADATION OF CARBON PHENOLIC

4.1 Background

The objective of Test Case 2 should be to model the pyrolysis progress versus time through a carbon phenolic ablator and to determine its thermal and ablative properties. In the case of carbon phenolic, whatever the density is, similar figures to Figure 1 may be obtained for varying pyrolysis gas blowing rates [2]. In order to better distinguish between the different phenomena influencing the ablation process a step by step approach has been proposed [2].

Test Case 2 will be initiated using a simple lay-up made of quasi 1D with fibres normal to the surface and no cross weave. The experiments to be rebuilt will be with a low level of radiation and if possible with an inert atmosphere.

A critical review of the available data from the literature on carbon phenolic have shown that experimental data obtained in arc jet facilities is available for two materials: FM5055 [14] and NARMCO 4028 [15]. These two sets of experiments have been used by Ahn et al [5] to validate the ablation tool KCMA. The paper of Wakefield & Pitts [14] shows that the experiments were performed in air but with a consequent level of radiation. Series of tests were performed with radiative heat-flux of 2.3 MW/m^2 and 0.6 MW/m^2 . For the other material, series of tests were performed by Sutton [15] without significant level of radiation and some with a low fraction of oxygen. Since there is no experimental data found in the literature for the ablation of carbon phenolic in an inert atmosphere and that the experimental study of covers a wide range of test conditions and is reported with sufficient details, this study has been selected for the definition of Test Case 2.

In future evolution of this test case, experimental tests performed in the frame of EAWG or ESA research and technology activities for Earth high-speed re-entry conditions will be used.

4.2 Objective

The objective of the Test Case 2 is to rebuilt the experiments of Sutton [15] performed with the carbon-phenolic NARMCO 4028. The tests have already been rebuilt by Sutton [15] and Ahn & al [5]. The outcome of the rebuilding is the prediction of the recession and surface temperature versus experimental dynamic conditions (cold wall heat flux and wall pressure). This, for a wide range of physical conditions and a stagnation point configuration.

From the experimental results, a matrix of computational conditions has been defined to cover, as far as possible, a wide range of flow conditions in terms of heat-flux and stagnation pressure.

Computations for the rebuilding can be uncoupled (preferably) which requires a knowledge of the surface temperature or coupled, depending only on test conditions.

4.3 Inputs

The inputs have been defined using the experimental data for test conditions and material properties available in [15]. The input parameters have been chosen in order to insure the best possible

coverage of the different carbon-phenolic ablation regimes.

4.3.1 Geometry

Tests were performed for blunt and hemispheric noses. The last configuration is retained to define the test case. The hemispheric geometry of the test sample is shown in Figure 6. The hemispheric cylinder has a diameter of 2.54 cm. The sample is 3.81 cm long with a nose radius of 1.27 cm. The specimen was machined with the across-grain direction parallel to the axis of the specimen, the direction of the lowest thermal conductivity.

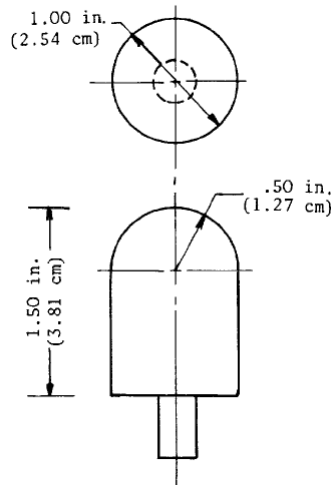


Figure 6: Geometry of the hemispheric samples [15].

| Stagnation pressure (atm) | Duration (s) | Nominal total enthalpy (MJ/kg) | Heat-flux (MW/m^2) | Surface temperature (K) | Mass fraction of oxygen |
|---------------------------|--------------|--------------------------------|-------------------------------|-------------------------|-------------------------|
| 0.31 | 30 | 25.05 | 14.19 | 3370 | 0.23 |
| 2.4 | 29.3 | 5.43 | 7.95 | 2480 | 0.23 |
| 8.62 | 15.2 | 2.55 | 6.13 | 2320 | 0.08 |
| 10.91 | 15.7 | 1.91 | 4.84 | 2135 | 0.09 |

Table 7: Test Case matrix from Sutton's experiments [15].

4.3.2 Test Matrix

The experimental campaigns carried out by Sutton for the carbon phenolic designated as NARMCO 4028 were conducted for a wide range of experimental conditions to obtain experimental data on char recession, thermal degradation of virgin material, back-surface temperature rise, surface temperature and observation of possible peculiarities of the material.

Tests were performed for an air atmosphere in two different facilities: the Langley 11-inch ceramic-heated tunnel and the Langley 20-inch hypersonic arc-heated tunnel. Many tests were performed for a

wide range of conditions in terms of total enthalpy, heat-flux, surface temperature, test duration and mass fraction of oxygen. The range of stagnation enthalpy was from 2.55 to 25.5 MJ/kg and the range of model stagnation pressure was from 0.07 to 11 atmospheres. Stagnation heating rates were obtained from 1.48 to 18.2 MW/m². The surface temperature was between 1870 and 3000 K. Some of the tests were carried out for air other a low mass fraction of oxygen (air-nitrogen mixture), some with an inert atmosphere of pure nitrogen.

From these tests, a matrix has been established by selecting the most relevant cases (full set of data, no length increase of the test sample). The test conditions on terms of stagnation pressure, duration, total enthalpy, cold wall heat-flux, surface temperature and mass fraction of oxygen are reported in Table 7. The range of stagnation pressure is from 0.035 up to 10.91 atmospheres and nominal enthalpy from 1.91 up to 25.05 MJ/kg. The corresponding range of surface temperature was between 2000 and 3000 K. There was a low radiation environment for the tests without significant radiative heating rate. The first and the last set of conditions from Table 7 were numerically rebuilt by Sutton.

| Stagnation pressure (atm) | Recession (cm) | Char thickness (cm) | Char mechanical removal |
|---------------------------|----------------|---------------------|-------------------------|
| 0.31 | -0,157 | 0.71 | No |
| 2.4 | -1,138 | --- | Yes |
| 8.62 | -0,091 | 0.46 | Yes |
| 10.91 | -0,483 | 0,33 | Yes |

Table 8: Sutton's test results [15].

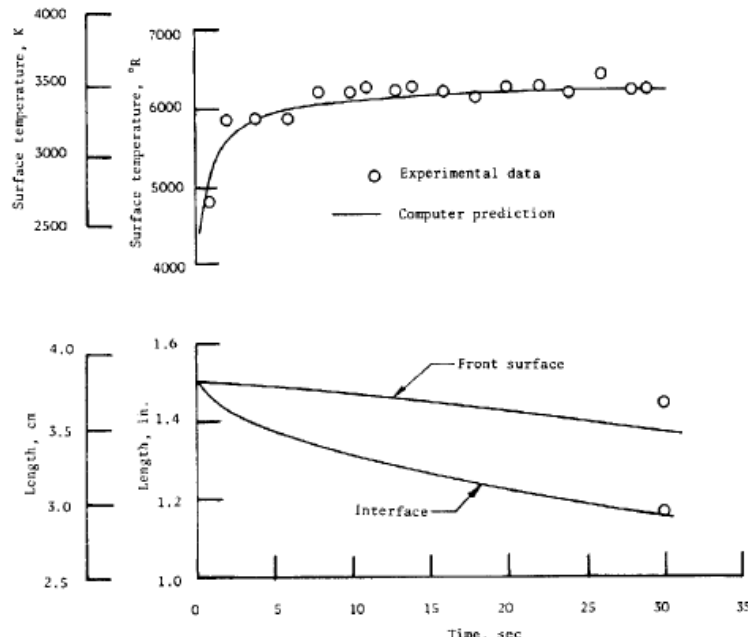


Figure 7: Recession and surface temperature as function of time for the test with air at the stagnation pressure of 0.31 atmosphere.

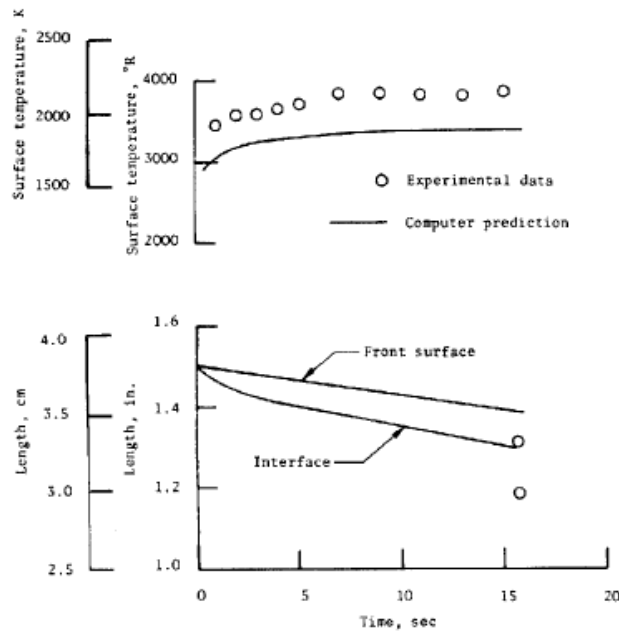


Figure 8: Recession and surface temperature as function of time for the test with air at the stagnation pressure of 10.91 atmospheres.

| t(s) | T(°K) |
|-------|-------|
| 0,71 | 2672 |
| 2,01 | 3254 |
| 3,78 | 3254 |
| 5,91 | 3280 |
| 8,04 | 3466 |
| 9,93 | 3439 |
| 11,11 | 3492 |
| 13,01 | 3466 |
| 13,95 | 3492 |
| 16,08 | 3466 |
| 18,09 | 3413 |
| 20,10 | 3492 |
| 22,23 | 3519 |
| 24,12 | 3466 |
| 26,01 | 3571 |
| 27,91 | 3479 |
| 29,09 | 3492 |

Table 9: Time evolution of the surface temperature for the test with air at the stagnation pressure of 0.31 atmosphere.

| | | | | | | | | | | |
|-------|------|------|------|------|------|------|------|------|------|------|
| T(°K) | 1912 | 2003 | 2016 | 2041 | 2067 | 2145 | 2158 | 2145 | 2145 | 2171 |
| t(s) | 1,1 | 2,2 | 3,3 | 4,4 | 5,6 | 7,8 | 10 | 12,2 | 14,4 | 16,6 |

Table 10: Time evolution of the surface temperature for the test with air at the stagnation pressure of 10.91 atmospheres.

4.3.3 Experimental Data

All test data was obtained at stagnation point for steady state conditions. The convective cold wall heat flux was related, to enthalpy by the correlation of Fay and Riddell [7]. Surface temperatures indicated in Table 7 have been measured for steady-state conditions. Char thickness has been measured at end of exposure time and after cool down, however an accurate definition of this parameter was not provided.

Transient results for the surface temperature are also available for the tests performed at 0.31 and 10.91 atmospheres. The measured values are reported in Table 9 and Table 10 and plotted in Figure 7 and Figure 8.

| Element | % in weight |
|----------|-------------|
| Carbon | 83.63 |
| Oxygen | 10.79 |
| Hydrogen | 3.44 |
| Nitrogen | 0.38 |
| Ash | 0.56 |

Table 11: Elemental composition of Narmco 4028.

| Property | Narmco 4028 |
|---|-----------------------|
| Density of virgin material (kg/m ³) | 1392 |
| Heat of pyrolysis (MJ/kg) | 0.465 |
| First frequency factor (kg/m ³ .s) | 4.7×10^{16} |
| First activation energy (MJ/mole) | 0.204 |
| Second frequency factor (kg/m ³ .s) | 4.96×10^{14} |
| Second activation energy (MJ/mole) | 0.209 |
| Porosity | 0 |
| Emissivity | Not Available |

Table 12: Properties of carbon-phenolic Narmco 4028 used by Sutton.

4.3.4 Material properties

NARMCO 4028 is a composite of 50 % by weight of carbon fibres and 50 % of phenolic resin. An elemental chemical analysis for the non-degraded material is given in Table 11. The values retained for the thermal properties are displayed in Table 12.

The tests performed by Sutton were rebuilt numerically. The thermal properties used for this rebuilding are retained here for the Test Case definition. The porosity was essentially zero since bulk and true densities were similar [16]. The nominal density of the virgin material measured was 1392 kg/m³. There is a discrepancy between measurements of char density in [15] and [16]. In [16] a char density of 1125 kg/m³ is given for char formed in a furnace and 1185 kg/m³ for a plasma jet. Sutton has measured a char density of 1185 kg/m³ for a furnace and densities from 913 to 1089 kg/m³ from several test models in a plasma jet. A value of 993 kg/m³ was retained for the numerical rebuilding and will be also used for the test case.

The heat of pyrolysis was determined by Sutton from measured differential thermal analysis data, the value of 0.465 MJ/kg seems to be low [17] but this is the only available data. The rate constants for

the thermal degradation such as the first and second frequency factors and the first and second activation energy (see Table 12) of the virgin material were determined from measured gravimetric data.

| T (K) | Cp (J/kg/K) |
|-------|-------------|
| 256 | 990 |
| 311 | 1220 |
| 367 | 1330 |
| 422 | 1390 |
| 477 | 1450 |
| 533 | 1510 |
| 589 | 1560 |
| 644 | 1620 |
| 700 | 1680 |
| 811 | 1800 |

Table 13: Values of the heat capacity for the Narmco 4028 (virgin).

| T (K) | Cp (J/kg/K) | Cp(gas) (J/kg/K) |
|-------|-------------|------------------|
| 278 | 1000 | 3,14 |
| 556 | 1380 | 4,18 |
| 811 | 1610 | 6,28 |
| 1089 | 1860 | 8,36 |
| 1366 | 2010 | 4,18 |
| 1645 | 2060 | 4,18 |
| 1923 | 2110 | 4,18 |
| 2200 | 2150 | 4,18 |
| 2478 | 2170 | 7,32 |
| 2756 | 2190 | 10,47 |
| 3030 | 2210 | 18,85 |
| 3311 | 2240 | 31,4 |
| 3590 | 2260 | 39,75 |
| 3867 | 2280 | 41,84 |

Table 14: Values of the heat capacities for the char material and the pyrolysis gas for the Narmco 4028.

Specific heat and thermal conductivity for the virgin and char materials are taken from [15] and [16] respectively. The values of specific heat for virgin and char materials are reported in Table 13 and Table 14. The value of the thermal conductivity measured by Engelke & al [16] are listed in Table 15 and Table 16.

| T(K) | 255 | 310 | 366 | 421 | 477 | 533 | 589 | 644 | 678 |
|----------|------|------|------|------|------|------|------|------|------|
| k(W/m/S) | 0,74 | 0,90 | 1,02 | 1,12 | 1,21 | 1,26 | 1,27 | 1,22 | 1,16 |

Table 15: Values of the thermal conductivity measured in the fibre direction for the virgin material [16].

| T(K) | 825 | 1075 | 1338 | 1672 | 1964 | 2240 | 2644 | 2894 |
|----------|------|------|------|------|------|------|-------|-------|
| k(W/m/s) | 5,29 | 5,61 | 5,92 | 4,67 | 7,16 | 9,34 | 17,44 | 21,18 |

Table 16: Values of the thermal conductivity measured in the fibre direction for the char material [16].

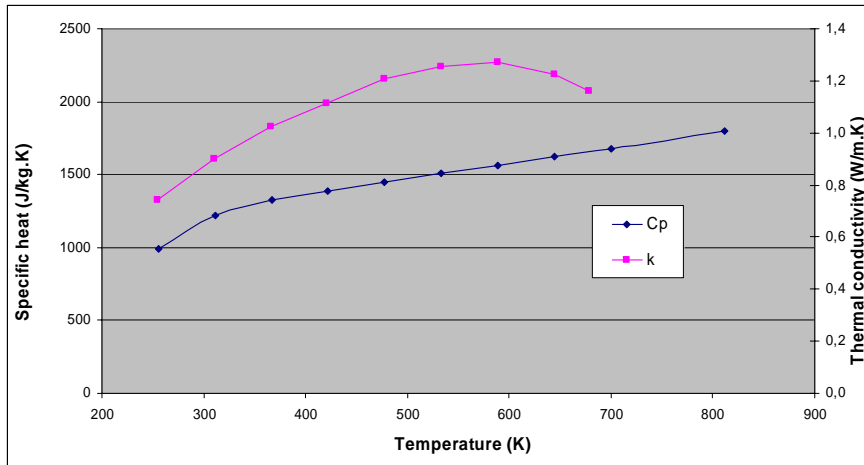


Figure 9: Distributions of specific heat and thermal conductivity as function of temperature for Narmco 4028 (virgin material).

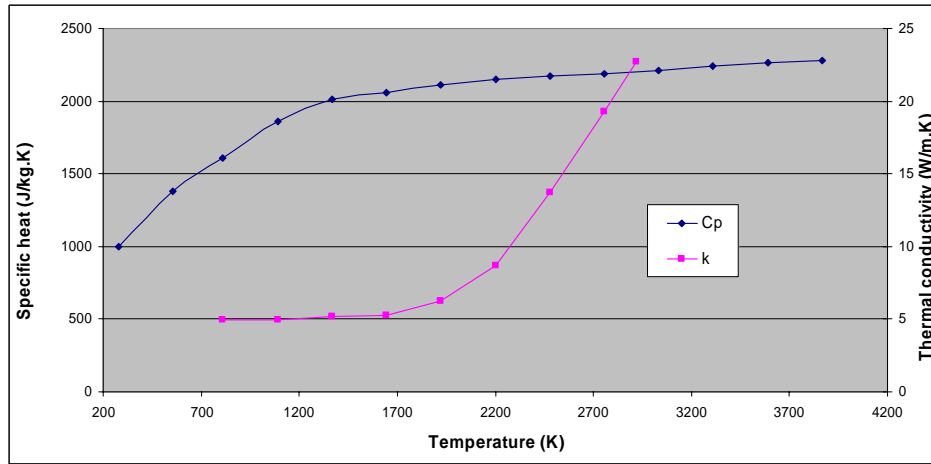


Figure 10: Distributions of specific heat and thermal conductivity as function of temperature for Narmco 4028 (char material) measured in [16].

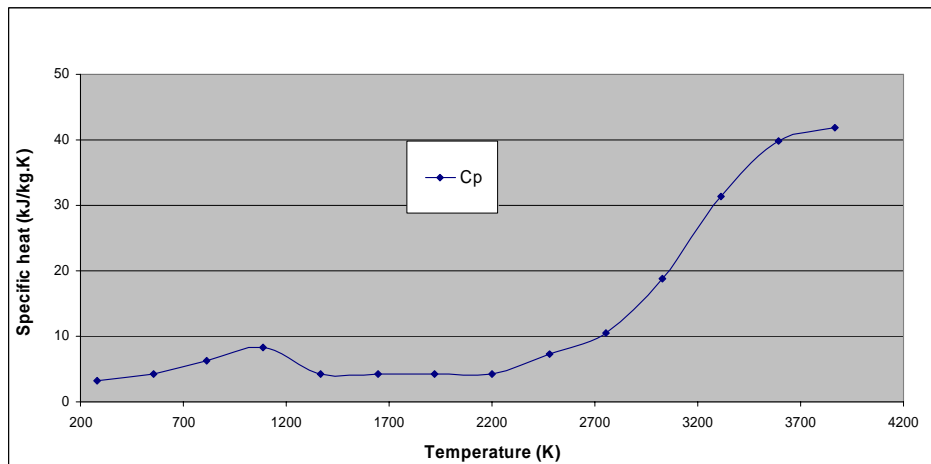


Figure 11: Distribution of the specific heat of the pyrolysis gases as function of temperature for Narmco 4028 computed by Sutton.

The corresponding distributions for the thermal conductivity and the specific heat are plotted in Figure 9 for the virgin material and Figure 10 for the char material. The specific heat of the pyrolysis gas, determined by Sutton from chemical equilibrium calculations, is also plotted in Figure 11. The determination using calculations did not account for char deposition.

The emissivity of the char is taken from [16]. The different values of the corresponding variables are listed in Table 17.

| Property | Narmco 4028 (char) |
|------------------------------|--------------------|
| Density (kg/m ³) | 993 |
| Emissivity | 0.7 |
| Porosity | 20% |

Table 17: Properties for the char material used by Sutton.

For Test Case 2 computations with this data are mandatory. Comparisons with other empirical or semi-empirical correlations are encouraged.

4.3.5 Chemical Kinetics

For Test Case 2, mass fraction of the different component of air atmosphere (O, N, N₂, O₂, NO) will be considered to be at equilibrium.

For fully coupled calculations using a CFD code accounting for non equilibrium the chemical model to be used will be the one proposed by Park et al [12].

4.4 Output

The ablation process is strongly driven by the surface temperature depending on test/entry conditions. This variable depends on the coupling between the flow conditions and the material behaviour. Nevertheless, in a first step it appears suitable to displays the ablation rate as function of surface temperature and wall pressure (as done in Figure 1) and/or cold wall heat flux and wall pressure.

For the numerical rebuilding, surface solutions can be empirical, equilibrium/transfer coefficient, coupled boundary layer or Navier-Stokes solutions. In further activities full kinetics non-equilibrium solutions can be considered as most suitable to compare with detailed modern spectral measurements.

Outputs should contain surface species, reactions and mole fraction profiles from the surface if CFD calculations have been performed, in Excel sheet format.

The results of the calculations for each of the mandatory cases should also be under the form of an Excel sheet containing for each case all used inputs: At least, wall heat flux and stagnation pressure and if used as inputs surface temperature; and as outputs: At least surface recession and if not used as input surface temperature (steady and unsteady).

Model details should be provided when possible: i.e. underlying databases, and methodology. Assumptions made in transport properties for all methods should be stated.

5 ANNEXES

5.1 Critical Literature Review of ATJ Graphite's data

A preliminary review of the literature data available and elements of interest in the objective of the numerical rebuilding of graphite experiments has been done [3] for the 3rd EAWG meeting. This review was based on a previous literature survey [18] performed on TPS materials by Fluid Gravity Engineering in 2003, which has been updated and completed when possible. Here, this preliminary review is used for the critical review in order to achieve the selection process between the available sets of data.

According to Havstad & Ferencz [19] despite the large number of experimental ablation studies in the open literature, many done with varying types of graphite, few were reported with sufficient details to be reproduced. The preliminary review has shown that ATJ graphite was the material with the most complete sets of data, as a consequence this material was chosen to build Test Case 1.

According to [18] and [19] the more extensive efforts were reported by Maahs [6], Baker et al. [20], Lundell & Dickey [21], Wakefield & Peterson [10], and in the Passive Nosetip Technology Program (PANT) [22,23]. From this list, the studies performed by Baker et al. [20] and in the frame of the PANT were not retained due to the difficulty to access to these results, while the works of Auerbach et al. [24] have been added. In order to build Test Case 1, the most complete sets of data available in the literature have been reviewed in details. The corresponding studies are those carried out by,

- Lundell & Dickey [21];
- Havstad & Ferencz [19];
- Auerbach et al. [24];
- Maahs [6,25];
- Wakefield & Peterson [10].

The experimental tests of Lundell & Dickey [21] are well documented, nevertheless the surface temperatures reported in this paper do not permit to cover the three ablation regimes shown in Figure 1. The range of surface temperature covers the diffusion limited and the sublimation regime but not the ablation regime dominated by the surface kinetics that is obtained for surface temperatures below 1500 K.

Havstad & Ferencz [19] have extensively investigated the surface kinetics including CN and CO formation, C₁-C₃, C₅ and C₇ sublimation. Correlations have been proposed for these phenomena that have been validated using PANT experimental data. The range of pressure in the PANT measurements extends up to 250 atm which is much higher than the pressure range retained for the test case (10 atm at the maximum). From the PANT results shown, only the sublimation regime could be covered.

The study of Auerbach et al. [24] was more focused on the graphite porosity. This author gives a

distribution of the recession rate versus time for ATJ graphite but with little details on the experimental conditions.

Maahs [6] investigated the performance of several materials including two graphites: one pyrolytic and one polycrystalline (ATJ graphite). The experimental results have allowed the development of empirical correlations for the mass loss rate as function of surface temperature and pressure. The experimental conditions are well described and the sublimation and diffusion limited regimes well covered, whereas the lower range of temperature and pressure is at the limit of the surface kinetics mode.

The same author [25] carried out an investigation on the effects of material properties on the behaviour of 45 different commercial brands of artificial graphite. It was found that the most significant factors affecting graphite performance were the maximum grain size, density, ash content, thermal conductivity and mean pore radius. For optimal performance the grain size should be small, density and thermal conductivity high, ash content low, and the mean pore radius large. This study was performed for only one set of experimental conditions corresponding to the diffusion limited regime.

The results of Wakefield & Peterson [10] cover both diffusion limited and sublimation modes. However, the set of data is not complete for defining a test case. Some data, such as the freestream velocity, the enthalpy and the test duration time is missing. Moreover, most of the tests were performed with a high level of radiative heating rates.

From this critical review of the available data it has been decided to propose a test case based on the results available in the NASA report of Maahs [6], which appears to be the most complete. However, a gap is existing in the experimental data with little material covering the surface kinetics regime. This could be filled by defining future experiments to be performed in the frame of the working group activities.

5.2 Maah's analysis of his own experiments

Measurements were performed for the different test conditions of Table 1 for the surface temperature, the total recession and the mass-loss-rate. The distributions of the mass-loss-rate and surface temperature as function of the stagnation pressure are plotted in Figure 4.

The mass loss rate and the surface temperature measured for a pressure of 0.6 atm are higher than for a pressure of 2 atm. The surface temperature is close to 3400 K. At this level of temperature, the vapour pressure of carbon has been variously reported to be between 0.005 atm and 0.5 atm. As a consequence, this increase in the mass-loss rate might be due to the contribution of sublimation.

Maahs [6] has advanced an argument to demonstrate that the mass-loss rate of carbon is not diffusion limited at the conditions of the presents tests. According to the concept of a diffusion limited rate, the mass loss rates for the material which are diffusion limited must be the same. But Figure 4 clearly shows that the mass loss rate of ATJ graphite differs appreciably. Experiments shown this tendency for four different graphites, as a consequence it seems obvious that the rates were

dependent on the carbon type and, hence, on chemical kinetics. From this conclusion and keeping in mind Figure 1 it is difficult to conclude that the surface kinetics regime is or is not covered. The comparison between the different rebuilding of the test cases and the synthesis of the different contributions might bring the solution of this point.

Another peculiar phenomenon in Figure 4 is the evolution of the mass loss rate at high pressure. From the experimental data at 15 atm, two rates were determined: one slow rate indicated by the continue line and one fast rate with the dashed line. For the test at high pressure (15 atm), shortly after the graphite sample was inserted into the test chamber, it began to recede at nearly a constant rate, but soon after its recession rate has almost tripled. For Maahs, this increase in the recession rate is probably associated with the fact that the samples erode their originally hemispherical noses and then become conical as shown in Figure 3. The slower rate may be associated to the erosion of a hemispheric nose while the faster rate can be thought as corresponding to the erosion of a conical nose. If the slow rate is retained as the recession value for an hemispheric shape, then for pressures higher than 2 atm the mass loss rate has a linear evolution.

The removal of ATJ graphite for the high-pressure condition was accompanied by considerable mechanical removal of particulate matter.

From the experimental results for the mass-loss rate \dot{m} , Maahs [6] has extracted the following empirical correlation:

$$\dot{m} = A e^{B/T} p_o^C \quad (5.1)$$

where p_o is the stagnation pressure, T the temperature and A, B and C a set of empirical constants. Two sets of empirical constants have been extracted using the test performed at 15 atm, one for the slower recession rate, the other for the faster rate. The different values of the constants are listed in Table 18.

| Rate | A | B | C | Average residual % | Maximum residual % |
|--------|-------|-------|-------|--------------------|--------------------|
| Slower | 0.059 | -3050 | 0.411 | 8.1 | 22.9 |
| Faster | 0.217 | -6745 | 0.761 | 18.6 | 73.4 |

Table 18: Values of the constants, A, B and C for the slower and faster rates respectively.

The average and maximum residuals are the average and maximum differences between the experimental data and the values predicted using equation (5.1) respectively.

5.3 Critical Literature Review for Carbon phenolic

A preliminary review of the literature data available and elements of interest in the objective of the numerical rebuilding of carbon-phenolic ablation experiments has been done [3] for the 3rd EAWG meeting. Here, this preliminary review is used as input for the critical review in order to achieve the

selection process between the available sets of data.

Most of the data available for carbon-phenolic ablation are flight data gathered during Pioneer-Venus and Galileo missions [26-27-28]. The carbon phenolic used for these heat-shields was referenced as FM-5055 and its properties of this material like thermal conductivity and heat capacity are also available [28]. A set of results is also available for the TPS testing of Galileo front shield [29]. The flight data recovered during the missions has been analysed during post-flight analysis with some numerical rebuilding [5-28-30-31]. Jupiter and Venus entries are characterized by high levels of radiative fluxes which makes the assessment of ablation more complex. Since in a first step Test Case 2 has to be defined for a low radiative environment this flight data will not be used.

Some investigations have also been performed on the FM5055 for the Rosetta programme [32] with the selection of carbon phenolic with a 0° lay-up carbon fibre angle. Experimental results have shown a material delamination in small sample tests due to the poor interlaminar strength and high gassing. A set of material properties on the material used for the tests is available [18], it includes emissivities, densities, thermal conductivity and specific heat for virgin and char material as well as the pyrolysis gas cooling efficiency. However, the experimental investigations were performed for only two points which is a very limited range for the definition of a test case.

Two sets of experiments have been used by Ahn et al to [5] validate the ablation tool KCMA. These two sets are the experimental results obtained in arc jet facilities on carbon-phenolics FM5055 and NARMCO 4028 by Wakefield & Pitts [14] and Sutton [15] respectively. The paper of Wakefield & Pitts shows that the experiments were performed in air but with a consequent level of radiation. Series of tests were performed with radiative heat-flux of 2.3 MW/m² and 0.6 MW/m².

Since there is no experimental data found in the literature for the ablation of carbon phenolic in an inert atmosphere and since the experimental study of Sutton [15] covers a wide range of test conditions and is reported with sufficient details, this study has been selected for the definition of Test Case 2.

5.4 Sutton's experiments

The experimental campaigns carried out by Sutton for the carbon phenolic designated as Narmco 4028 were conducted for a wide range of experimental conditions. Tests have been performed for a wide range of experimental conditions to obtain experimental data on char recession, thermal degradation of virgin material, char retention, back-surface temperature rise, surface temperature and observation of possible peculiarities of the material. The effects of hole patterns in the material and the effects of injecting water into the flow-field were also evaluated. Influence of fibre orientation was also investigated. This material has been used for the heat-shield in the nose region for some re-entry flight vehicles of the RAM (Radio Attenuation Measurement) project. This project was investigating the blackout of radio communications encountered during Earth atmospheric re-entry.

Tests were performed for an air atmosphere in two different facilities: the Langley 11-inch ceramic-heated tunnel and the Langley 20-inch hypersonic arc-heated tunnel. The test conditions in terms of

total enthalpy, heat-flux, surface temperature, test duration and mass fraction of oxygen for an hemispheric shape and a parallel direction of the fibres are reported in Table 19. The range of stagnation enthalpy was from 2.55 to 25.5 MJ/kg and the range of model stagnation pressure was from 0.07 to 11 atmospheres. Stagnation heating rates were obtained from 1.48 to 18.2 MW/m². The surface temperature was between 1870 and 3000 K. Some of the tests were carried out for air other a low mass fraction of oxygen (air-nitrogen mixture), some with an inert atmosphere of pure nitrogen.

| Stagnation pressure (atm) | Duration (s) | Nominal total enthalpy (MJ/kg) | Heat-flux (MW/m ²) | Surface temperature (K) | Mass fraction of oxygen |
|---------------------------|--------------|--------------------------------|--------------------------------|-------------------------|-------------------------|
| 0.07 | 30 | 25.52 | 7.72 | 3090 | 0.23 |
| 0.31 | 30 | 25.05 | 14.19 | 3370 | 0.23 |
| 0.43 | 30 | 3.59 | 1.48 | 1870 | 0.23 |
| 0.6 | 30 | 25.52 | 18.16 | 3700 | 0.23 |
| 1.08 | 20 | 12.76 | 12.37 | --- | 0.08 |
| 1.38 | 30 | 3.48 | 3.72 | --- | 0.23 |
| 2.4 | 29.3 | 5.43 | 7.95 | 2480 | 0.23 |
| 2.5 | 20 | 4.41 | 6.47 | 2595 | 0.08 |
| 2.91 | 30 | 3.48 | 5.62 | --- | 0.23 |
| 6.05 | 20 | 2.55 | 5.11 | 2323 | 0.08 |
| 6.13 | 30 | 2.55 | 5.18 | 2145 | 0.23 |
| 6.24 | 15.2 | 2.55 | 5.28 | 2390 | 0.12 |
| 8.62 | 15.2 | 2.55 | 6.13 | 2320 | 0.08 |
| 10.72 | 20.2 | 2.55 | 6.88 | 2630 | 0.23 |
| 10.78 | 30.7 | 2.55 | 6.88 | 2100 | 0 |
| 10.91 | 15.7 | 1.91 | 4.84 | 2135 | 0.09 |
| 11 | 20 | 2.55 | 6.92 | 2310 | 0.1 |

Table 19: Sutton's test experimental conditions [15].

Tests were performed for blunt and hemispheric noses. The last configuration was retained to define the test case. During the tests, the stagnation-point length change, the char thickness and the approximate equilibrium stagnation-point temperature were measured. The results for the char thickness and the length change are reported in Table 20. The measured surface temperatures are given in Table 19. For some of the tests, there was a measurable expansion of the material which offset the recession. In many of the tests, the length of the model was greater after the test than before. The attempts made by Sutton to correlate the expansion with various parameters were unsuccessful. It seems this effect is induced by the fibre orientation [15].

The char thicknesses are given in Table 20 only for the tests where the thermal degradation could be attributed to one dimensional heat conduction. Good recession rate data for the chemical removal of the char were not obtained in the Sutton's tests. At the higher pressure conditions the mechanical

char removal was superimposed on the chemical removal.

| Stagnation pressure (atm) | Recession (cm) | Char thickness (cm) | Char mechanical removal |
|---------------------------|----------------|---------------------|-------------------------|
| 0.07 | 0,086 | 0.71 | No |
| 0.31 | -0,157 | 0.71 | No |
| 0.43 | -0,015 | 0.61 | No |
| 0.6 | -0,29 | --- | No |
| 1.08 | 0,041 | --- | No |
| 1.38 | -0,079 | 0.66 | No |
| 2.4 | -1,138 | --- | Yes |
| 2.5 | 0,094 | --- | No |
| 2.91 | -0,404 | 0.51 | Yes |
| 6.05 | 0,056 | 0.35 | Yes |
| 6.13 | 0,127 | --- | Yes |
| 6.24 | -0,023 | 0.56 | Yes |
| 8.62 | -0,091 | 0.46 | Yes |
| 10.72 | -1,316 | 0.41 | Yes |
| 10.78 | 0,17 | --- | No |
| 10.91 | -0,483 | 0,33 | Yes |
| 11 | -0,606 | --- | Yes |

Table 20: Sutton's test results

A large number of tests were affected by char mechanical removal, they are indicated in Table 20. This phenomenon was observed to occur at certain test conditions for air or air-nitrogen mixtures but not for pure nitrogen. It was not observed in air mixtures at stagnation pressures lower than 2 atmospheres. At stagnation pressures higher than 6 atmospheres, mechanical char removal occurred whenever oxygen was present. For air environment (oxygen mass fraction of 0.23 in Table 19), mechanical char removal occurred at stagnation pressures as low as 2.4 atmospheres. Char removal was not induced by a mechanical effect such as aerodynamic shear since it was not observed during test with nitrogen at a stagnation pressure as high as 11 atmospheres. If we consider the char as a porous media then an inflow of gas from the boundary layer containing oxygen is possible. This inflow could oxidize the char and weaken the interior structure of the char to such an extent that mechanical char removal by aerodynamic shear becomes possible.

The experiments were numerically rebuilt by Sutton. Because of this mechanical removal (see Figure 12) and material expansion, Sutton was not able to obtain a good experimental comparison with chemical removal theories for the char even though the model surface temperatures were in the range usually associated with diffusion-controlled oxidation and sublimation of the char. Recently, Ahn & al

[5] have performed a test rebuilding using the KCMA software. They achieved a good agreement with the experimental data for the prediction of the surface temperature and the recession length for a stagnation pressure of 0.31 atmosphere and enthalpy of 25.05 MJ/kg and a cold wall heat-flux of 14.2 MW/m².

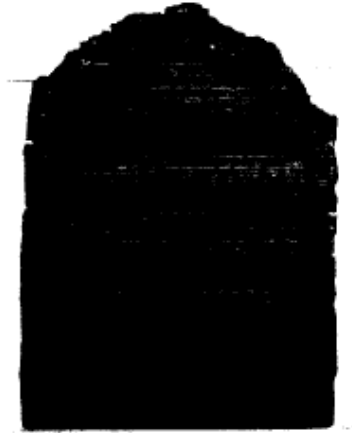


Figure 12: Char removal of an hemispheric model for a test a 11.26 atm.

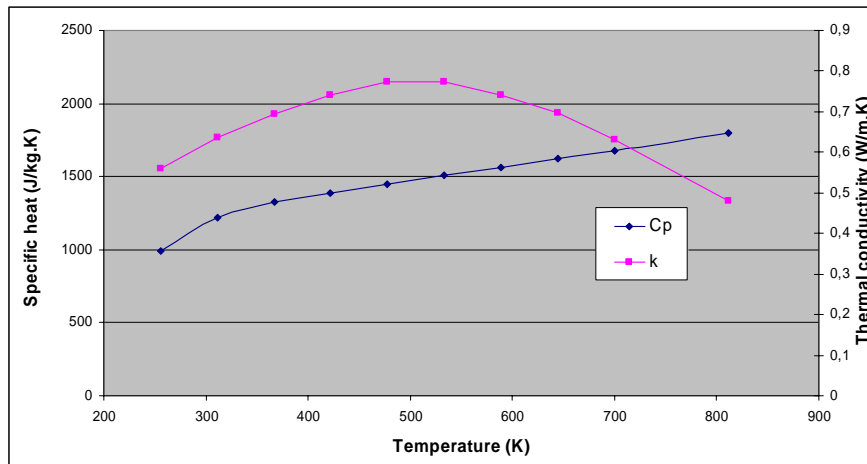


Figure 13: Distributions of specific heat and thermal conductivity as function of temperature used by Sutton for Narmco 4028 (virgin material).

5.5 Sutton's numerical rebuilding

Sutton has performed a numerical rebuilding of his own tests. The thermal properties used for this rebuilding are retained here for the Test Case definition excepted the thermal conductivity. The selected thermal conductivities are based on the data of [16] for heat flow at the model stagnation region for perpendicular-fibre and shingled-fibre orientation of the Sutton's study. According to Sutton the thermal conductivity of the virgin material was taken from [16] while the thermal conductivity for the char is one-half the value given in [16] in the across fibre direction. The corresponding

distributions for the thermal conductivity and the specific heat for the virgin and char materials are plotted in Figure 10 and Figure 14. However in the study of Engelke et al [16], the thermal conductivity was not measured above 3030 K for the char material while Sutton provides data up to 3700 K. So, there is some doubts on the origin of the data used by Sutton. As a consequence for the definition of Test Case 2, it is proposed to use the set of data measured in the direction parallel to the fibres by Engelke et al [16].

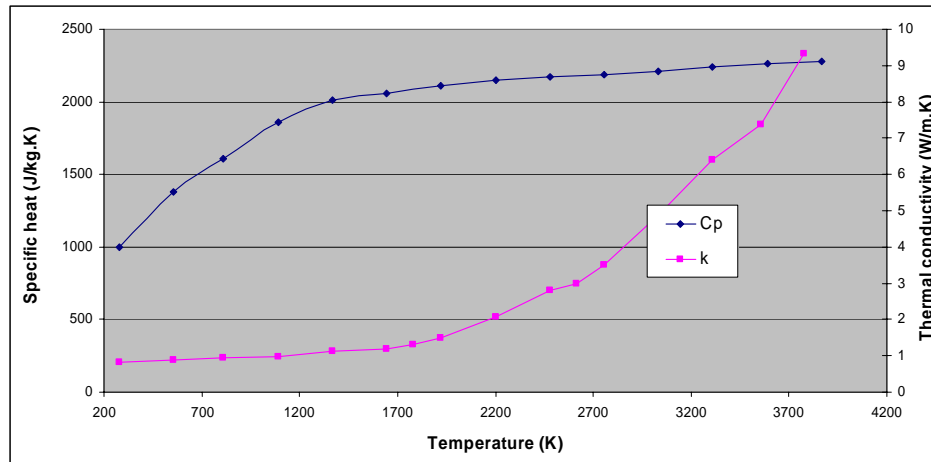


Figure 14: Distributions of specific heat and thermal conductivity as function of temperature used by Sutton for Narmco 4028 (char material).

Other material properties used by Sutton were heat of combustion of the char selected as a 10 to 20% increase over the value of formation of carbon monoxide formed from graphite and oxygen. The value of the heat of sublimation of the char was an average value for the sublimation of graphite. The char surface kinetics were chosen as equal of the slow kinetics for graphite and taken from [33]. The different values of the corresponding variables are listed in Table 17. This is a very crude model for carbon ablation [17] that has not been retained.

| Property | Narmco 4028 (char) |
|--|--------------------|
| Heat of combustion (MJ/kg) | 11.82 |
| Heat of sublimation (MJ/kg) | 20.88 |
| Frequency factor ($\text{kg/m}^3 \cdot \text{s} \cdot \text{atm}^{1/2}$) | 21.8×10^4 |
| Activation energy (MJ/mole) | 0.177 |
| Reaction order | 0.5 |

Table 21: Properties for the char material used by Sutton.

6 REFERENCES

- [1] Reynier, Ph., Ritter, H., Maraffa, L., "Ablation Working Group", ESTEC, Noordwijk, October 2005.
- [2] Smith, A., J., Ablation Working Group – Preliminary Identification of Test Cases 2nd Ablation Working Group Meeting, ESTEC, May 16, 2006;
- [3] Reynier, Ph., Preliminary test case definition for numerical rebuilding within the European Ablation Working Group, ESA Contract 065/2006, ISA-TN1-2006, Ingénierie et Systèmes Avancés, Nov. 2006.
- [4] Smith, A., J., FABL3 (User Manual) – A program for analysing charring ablation thermal protection systems, TN20/96 Issue 4, Fluid Gravity Engineering, May 2000.
- [5] Ahn, H.–K., Park, C., & Sawada, K., Response of heatshield material at stagnation point of Pioneer-Venus probe, *Journal of Thermophysics and Heat Transfer*, Vol. 16(3), pp. 432-439, 2002.
- [6] Maahs, H. G., Ablation performance of glasslike carbons, pyrolytic graphite, and artificial graphite in the stagnation pressure range 0.035 to 15 atmospheres, NASA TN D-7005, December 1970.
- [7] Fay, J. A., & Ridell, F. R., Theory of stagnation point heat transfer in dissociated air, *J. Aeronautical Science*, Vol. 25(2), pp. 73-85, Feb. 1958.
- [8] Reynier Ph., Skeleton for material database, Ingénierie et Systèmes Avancés, 3rd Ablation Working Group Meeting, Bordeaux, January 25-26, 2007.
- [9] Anon., Advanced Materials Technology. Hardware for Cryogenic to 6000 F and Above Environments. Super-Temp Corp.
- [10] Wakefield, R. M., & Peterson, D. L., Graphite ablation in combined convective and radiative heating, *Journal of Spacecraft and Rockets*, Vol. 10(2), pp. 149-154, 1973.
- [11] Williams, S. D., & Curry, D. M., Thermal Protection Materials - Thermophysical Property Data, NASA Reference Publication 1289, 1992.
- [12] Park, C., Jaffe, R. L., & Partridge, H., Chemical-Kinetic parameters of hyperbolic Earth entry, *Journal of Thermophysics and Heat Transfer*, Vol. 15, No.1, pp. 76-90, January-March 2001.
- [13] Ahn, H. K., & Park, C., Preliminary study of the MUSES-C reentry, AIAA Paper 97-0278, 1997.
- [14] Wakefield, R. M., & Pitts, W. C., Analysis of the heat-shield experiment on the Pioneer-Venus entry probe, AIAA Paper 80-1494, July 1980.
- [15] Sutton, K., An experimental study of a carbon-phenolic ablation material, NASA TN D-5930, Sept. 1970.
- [16] Engelke, W. T., Pyron, C. M., & Pears, C. D., Thermal and mechanical properties of a nondegraded and thermally degraded phenolic carbon composite, NASA CR-896, 1967.
- [17] Duffa, G., Remarks on Test Case Definition for numerical rebuilding within the European Ablation Working Group, 13 Aug. 2007.
- [18] White, T., & Parnaby, G., Thermal protection system materials and response correlations literature survey, CR036/03, Fluid Gravity Engineering, July 2003.
- [19] Havstad, M. A., & Ferencz, R. M., Comparison of surface chemical kinetic models for ablative reentry of graphite, *Journal of Thermophysics and Heat Transfer*, Vol. 16(4), pp. 508-515, 2002
- [20] Baker, R. L., Covington, M. A., & Rosenblatt, G. M., The determination of carbon thermochemical properties by laser vaporization, High Temperature Materials chemistry Symposium, electrochemical Society, Pennington, NJ, pp. 143-154, 1983.
- [21] Lundell, J. H., & Dickey, R. R., Ablation of ATJ graphite at high temperature, *AIAA Journal*, Vol. 11(2), pp. 216-222, 1973.

-
- [22] Wool, M. R., Passive Nosetip Technology (PANT) Program, ACUREX Corp., Final Summary Report, AD-A019 186, SAMSO-TR-75-220, Los Angeles, June 1975.
- [23] Shimizu, A. B., Ferrell, J. E., & Powars, C. A., Passive Nosetip Technology (PANT) Program, Vol. 12, Nosetip Transition and Shape Change Tests in the AFFDL 50 MW Rent Arc, ACUREX Corp., data Report, AD-A020 710, SAMSO-TR-74-86, Los Angeles, april 1974.
- [24] Auerbach, I., Lieberman, M. L., Lawson, K. E., Pierson, H. O., Effects of porosity in graphite materials on ablation in arc-heated jets, *Journal of Spacecraft & Rockets*, Vol. 14(1), pp. 19-24, January 1977.
- [25] Maahs, H. G., A study of the effect of selected material properties on the ablation performance of artificial graphite, NASA TN D-6624, March 1972.
- [26] Seiff, A., Kirk, D. B., Young, R. E., Blanchard, R. C., Findlay, J. T., Kelly, G. M., & Sommer, S. C., Measurement of thermal structure and thermal contrasts in the atmosphere of Venus and related dynamical observations; Results from the four Pioneer Venus probes, *Journal of Geophysical Research*, Vol. 85(13), pp. 7903-7933, 1980.
- [27] Milos, F. S., Galileo probe heat shield ablation experiment, *Journal of Spacecraft and Rockets*, Vol. 34(6), pp. 705-713, 1997.
- [28] Milos, F. S., Chen, Y.-K., Squire, T. H., & Brewer, R. A., Analysis of Galileo probe heatshield ablation and temperature data, *Journal of Spacecraft and Rockets*, Vol. 36(3), pp. 298-306, 1999.
- [29] Green, M. J., & Davy, W. C., Galileo probe forebody thermal protection, AIAA Paper 81-1073, 1981.
- [30] Park, C., & Tauber, M. E., Heatshielding problems of planetary entry, a review, AIAA Paper 99-3415, 1999.
- [31] Matsuyama, S., Ohnishi, N., Sasoh, A., & Sawada, K., Numerical simulation of Galileo probe entry flowfield with radiation and ablation, *Journal of Thermophysics and Heat Transfer*, Vol. 19(1), pp. 28-35, 2005.
- [32] Smith, A. J., Carbon phenolic ablation testing and analysis for high speed Earth return, In *Proceedings of 24th International Conference on Environmental Systems and 5th European Symposium on Space Environmental Control Systems*, June 1994.
- [33] Scala, S. M., The ablation of graphite in dissociated air. Part I: Theory., R62SD72, Missile and Space Division, General Electric, CO, Sept. 1962.